Microchimica Acta (2022) 189: 136
https://doi.org/10.1007/s00604-022-05239-z

ORIGINAL PAPER

Electrochemiluminescent determination of CYFRA21-1 serum levels using Ti-Fe–O nanotubes immunoassay

Qing Hua[1] · Feiyan Tang[1] · Xiaobin Wang[1] · Feng Luan[1] · Wenjie Sun[1] · Yuanyuan Liang[1] · Lihong Zhang[1] · Xuming Zhuang[1] · Chunyuan Tian[1]

Received: 20 December 2021 / Accepted: 20 February 2022 / Published online: 8 March 2022

Abstract

Prominent electrochemiluminescence (ECL) in Ti-Fe–O nanotube arrays (Ti-Fe–O NTs) with $K_2S_2O_8$ as the cathode coreactant is reported for the first time. Compared with pure titanium dioxide nanotubes (TiO_2 NTs), this heterojunction could effectively reduce the band gap, facilitate electronic transitions, and move the ECL potential to a positive direction. The ECL performance motivated the development of an ultrasensitive ECL immunosensor for detecting cytokeratin fragment 21–1 (CYFRA21-1). Magnetic beads loaded with conductive carbon black (CCB/MNTs) were used to efficiently quench the ECL signal of a Ti-Fe–O NTs electrode and were combined with an ECL immunoassay to realize sensitive detection of CYFRA21-1. Over a CYFRA21-1 concentration range of 1.0 pg·mL^{-1} ~ 100 ng·mL^{-1}, the change in the ECL signal was highly linear with the logarithm of the CYFRA21-1 concentration, and the limit of detection (LOD) was 0.114 pg·mL^{-1}. This ECL immunosensor was used to successfully determine the CYFRA21-1 content in serum. The recovery of CYFRA21-1 in actual serum was 88.6 – 104.4%, and the RSD was 1.4 – 3.0%. The coreaction solution used in this work was PBS (0.1 M, pH = 7.4) containing 0.05 M $K_2S_2O_8$, the scanning range was −1.0 – 0 V, the photomultiplier tube (PMT) was set to 750 V, and the scanning rate was 100 mV·s^{-1}.

Keywords Electrochemiluminescence · Ti-Fe–O nanotube arrays · CYFRA21-1 · Immunoassay

Introduction

Titanium dioxide nanotubes (TiO_2 NTs) have been widely used in solar cells, photocatalysis, biosensors, etc., due to their large specific surface area, environmental protection, and relatively low cost [1–5]. Recently, Oriol's group [6] reported the photoelectrocatalytic treatment of indigo carmine in an acidic aqueous solution using TiO_2 NTs as photoanodes with good results. Although the application of TiO_2 NTs to photoelectrochemical (PEC) and electrochemical (EC) fields has been extensively studied, the application of TiO_2 NTs to the field of electrochemiluminescence (ECL) has rarely been studied. The main reason for this lack of research is that the wide band gap (3.2 eV) of TiO_2 NTs makes it difficult to excite electrons, resulting in poor ECL performance. Generally, the band gap can be modified by methods such as dye sensitization [7], ion doping [8], metal deposition [9–11], and loaded nanomaterials [12–14].

The heterojunction of TiO_2 and Fe_2O_3 has attracted increasing attention because of good performance. This heterojunction has effectively reduced the band gap (2.2 eV), promotes the electronic transitions, and enhanced ECL property compared to TiO_2 NTs [15, 16]. The doping of Fe_2O_3 onto TiO_2 has been implemented in a sol–gel system [17]. However, Fe_2O_3 has not been able to be atomically doped onto TiO_2 in most studies [18]. Ti-Fe–O nanotubes (Ti-Fe–O NTs) have considerably extended the utilization of visible light owing to the unique tubular structure and uniform atom doping of these NTs. To the best of our knowledge, Ti-Fe–O NTs are a mature application in the field of lithium-ion batteries and PECs [18–20] but have rarely been reported for applications in the ECL field.

ECL has been widely used in the fields of biological sciences, immunoassays, and food analysis because of a high speed, low background noise, high sensitivity, and simple

✉ Xuming Zhuang
xmzhuang@iccas.ac.cn

✉ Chunyuan Tian
cytian@ytu.edu.cn

[1] College of Chemistry and Chemical Engineering, Yantai University, Yantai 264005, China

equipment [21–23]. Lung cancer has become one of the deadliest malignant tumors due to its high fatality rate [24]. Cytokeratin fragment 21–1 (CYFRA 21–1) can be used to detect non-small lung cancer cell markers. Due to its high specificity, it has been widely used in immunoassays and has become an important tool for the quantitative analysis of tumor markers [25, 26]. Therefore, it is of great significance to use Ti-Fe–O NTs as electrodes to target CYFRA21-1.

This article is the first report of ECL in Ti-Fe–O NTs with $K_2S_2O_8$ as the cathode coreactant; an immunosensor for detecting CYFRA21-1 was designed with a Ti-Fe–O NTs electrode as an ECL emitter, and the principle is shown in Scheme 1. Magnetic beads loaded with conductive carbon black (CCB/MNPs) were used as amplifying quenchers and combined with Ab2 to detect CYFRA21-1 in serum. Experimental results showed that a Ti-Fe–O NTs electrode in a $K_2S_2O_8$ coreactant produced ECL signals with high stability and reproducibility.

Experimental

Reagents and chemicals

CYFRA21-1 and cytokeratin 19 fragment antigen 21–1 antibodies (antiCYFRA21-1) were obtained from Shanghai Linc-Bio Science Co., Ltd. Prostate protein antigen (PSA) and carcinoembryonic antigen (CEA) were obtained from the Huayang Zhenglong Biochemical Products Research Office. Bovine serum albumin (BSA) and tetracycline-BSA (TC-BSA) were purchased from Shenzhen Kejie Bio Co., Ltd. N-(3-dimethylaminopropyl)-N'-ethyl-carbodiimide hydrochloride (EDC) and N-hydroxysuccinimide (NHS) were purchased from Shanghai Sinopharm Chemical Reagent Co., Ltd. HIV-1 Tat protein was purchased from Shanghai Sangon Biotech Co., Ltd. Ulinastatin (UTI) was obtained from Eddie Pharmaceutical Co., Ltd. CCB was purchased from Nanjing Xianfeng Nano Co., Ltd. Affimag magnetic microspheres (MNPS) were obtained from the Tianjin Beisle Chromatography Technology Development Center. Hydrofluoric acid (HF) was purchased from Yantai Sanhe Chemical Reagent Co., Ltd. Oxalic acid (OA) was purchased from Tianjin Guangcheng Chemical Reagent Co., Ltd. Absolute ethanol (C_2H_5OH) was obtained from Sinopharm Chemical Reagent Co., Ltd. Ti-Fe alloy plates were purchased from Yinuo Metal Materials Co., Ltd. A Ti-Fe alloy plate was cut into 6×0.7 cm pieces (Fe $\leq$ 0.3).

Instrumentation

The ECL and other electrochemical properties were measured on an MPI-E ECL analysis system produced by Xi'an Raymine Analytical Instruments Co., Ltd. Scanning electron microscopy (SEM) was performed on an S-4800 electron microscope (Hitachi, Ltd., Japan). Energy dispersive spectroscopy (EDS) was carried out using an OXFORD Ultim Extreme. X-ray photoelectron spectroscopy (XPS) was carried out using a Thermo ESCALAB-250 (USA).

Preparation of an ECL biosensor

Ti-Fe–O NTs were successfully synthesized according to the literature [27]. The Ti-Fe–O NTs electrode was placed in 1 mL of PBS containing 3 mM OA, reacted for 5 h at 4 °C, and rinsed with ultrapure water and PBS. The OA-Ti-Fe–O NTs electrode was immersed in 1.0 mL of a solution containing 20 mg of EDC and 10 mg of NHS methyl imidazole to activate the carboxyl groups of OA at 25 °C for 1 h.

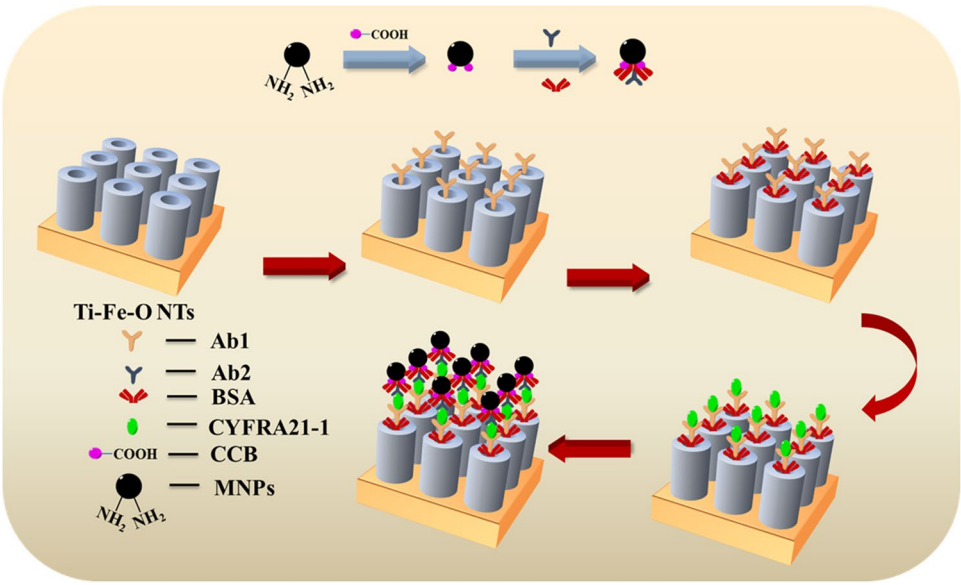

Scheme 1 Schematic of the Ti-Fe–O NTs for detecting CYFRA21-1

Washed with PBS to remove excess EDC and NHS on the electrode. Placed the electrode in Ab1 at 4 °C and assembled for 15 h. The Ti-Fe–O NTs electrode assembled with Ab1 was placed in a 3% BSA solution at 4 ℃ for 2 h to seal the non-specific active adsorption sites on the array electrode. The obtained electrode was labeled Ab1/Ti-Fe–O NTs.

The Ab1/Ti-Fe–O NTs were immersed in CYFRA21-1 at concentrations of 100 ng·mL^{-1}, 10 ng·mL^{-1}, 1 ng·mL^{-1}, 500 pg·mL^{-1}, 100 pg·mL^{-1}, 10 pg·mL^{-1}, and 1 pg·mL^{-1} and incubated at 37 °C for 1 h. The Ab1/Ti-Fe–O NTs bound to the antigen were labeled CYFRA21-1/Ab1/Ti-Fe–O NTs. The cells were further incubated with 1 mL of the Ab2/CCB/MNPs solution for 1 h at 25 °C. Finally, the cells were washed with ultrapure water and PBS and stored at 4 °C. The other conditions were as follows: the scanning potential was − 1.0 ~ 0 V, the scan speed was 100 mV·s^{-1}, and the strength of the photomultiplier tube was 750 V.

Results and discussion

Characterization of nanocomposites

The morphologies of the Ti-Fe–O NTs were first investigated using SEM (Fig. 1a). The results showed the material had a continuous porous nanotube structure. The inner diameter of the nanotubes was approximately 60 ~ 70 nm. The EDS results demonstrated the presence of Ti, O, and Fe (Fig. 1b). The atomic ratios of Ti, Fe, and O were 46.64%, 0.1%, and 53.26%, respectively.

The elemental composition and valence state of the synthesized Ti-Fe–O NTs were analyzed by XPS. The results showed the presence of elemental Ti, Fe, O, and C in the material. Figure S1A shows 4 distinct peaks at approximately 284.94, 459.42, 531.57, and 711.75 eV that were attributed to C 1 s, Ti 2p, O 1 s, and Fe 2p, respectively. We analyzed the Fe elemental peak, which is shown in Fig. S1B. The XPS Fe 2p spectrum exhibits two main peaks at approximately 711.84 and 723.72 eV, corresponding to Fe $2p_{3/2}$ and Fe $2p_{1/2}$, respectively, and confirming the presence of Fe^{3+} [18]. The satellite vibration peak of 715.98 eV further confirmed that the nanotubes contained Fe^{3+} [19, 28]. Given the multiple confirmations of the presence of Fe_2O_3, the obtained nanotubes were considered to be Ti-Fe–O NTs during the whole experiment.

Figure 2a shows the ECL performance of the pure TiO_2 NTs and Ti-Fe–O NTs electrodes in the $K_2S_2O_8$ coreactant solution. Compared with the electrode modified with pure TiO_2 NTs, the ECL intensity of the Ti-Fe–O NTs electrode was 5.7-fold higher, and the onset ECL potential was positively shifted to approximately 200 mV. The ECL intensity of the electrode modified with TiO_2 NTs and Ti-Fe–O NTs was measured under the action of a filter with a wavelength of 420 ~ 640 nm, and the results are shown in Fig. 2b. The maximum emission wavelength of the ECL emission peak was approximately 540 nm. Compared with the TiO_2 NTs electrode with a wavelength of 500 nm, the Ti-Fe–O NTs electrode exhibited a clear redshift, and the luminescent potential was positively shifted [27]. Compared to the TiO_2 NTs, the Ti-Fe–O NTs had a narrower band gap, which is consistent with the results in the literature [18], such that electrons in the Ti-Fe–O NTs were more easily excited to produce the ECL phenomenon.

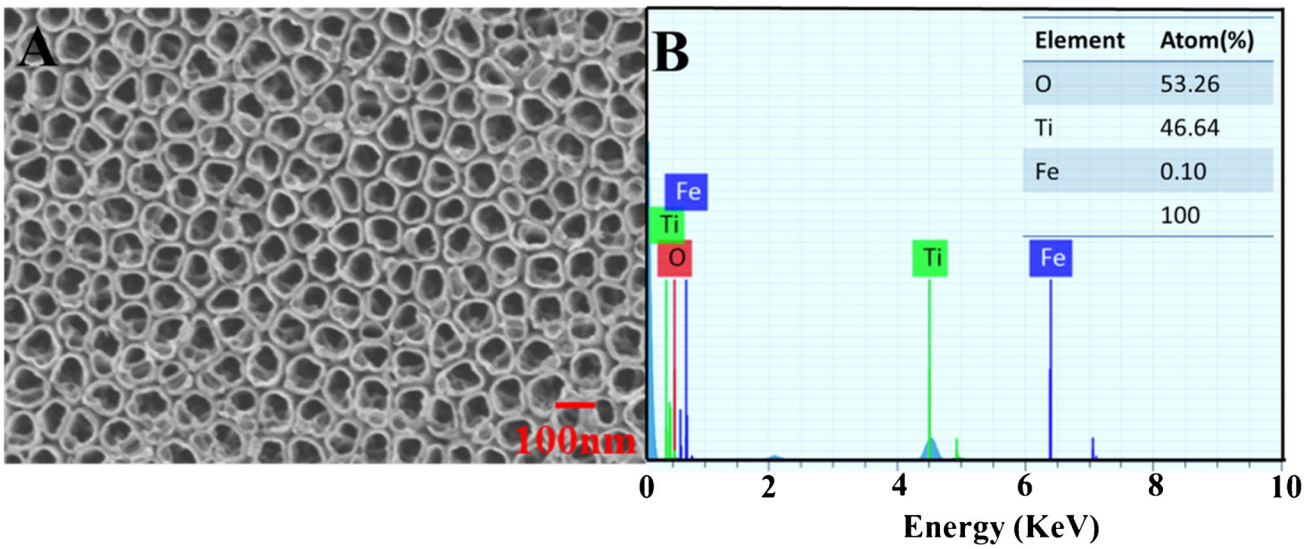

Fig. 1 **a** SEM image of Ti-Fe–O NTs (the scale in the SEM micrograph is 100 nm). **b** EDS of Ti-Fe–O NTs (elemental Ti, Fe, and O are present)

In order to further explore the performance of CCB/MNPs as quenching agents, the UV–vis absorption is shown in Fig. S2. It can be seen from the figure that there is a broad absorption peak in the wavelength range of 280 ~ 800 nm. This proved that CCB/MNPs were similar to blackbody materials. In addition, CCB was more environmentally friendly than common CdTe nanoparticles. Therefore, CCB/MNPs can be considered as a good quencher.

Optimization of experimental conditions

The pH of the coreactant significantly influenced the ECL of the Ti-Fe–O NTs electrode. Therefore, the pH of the $K_2S_2O_8$ coreactant was optimized, and the result is shown in Fig. S3. As the pH of the $K_2S_2O_8$ coreactant increased from 4 to 11, the ECL intensity first increased and then decreased. The ECL intensity had a maximum value at a $K_2S_2O_8$ coreactant pH of 7.4, which was hence chosen as the optimal detection condition in this study.

ECL behavior of Ti-Fe–O NTs

In a previous report on TiO_2 NTs [29], the ECL behavior of Ti-Fe–O NTs with $K_2S_2O_8$ as a coreactant was studied, and the following mechanism for inducing ECL was proposed.

$$S_2O_8^{2-} + e^- \rightarrow SO_4^{2-} + SO_4^{\cdot -} \quad (1)$$

$$SO_4^{\cdot -} \rightarrow SO_4^{2-} + h^+ \quad (2)$$

$$Ti - Fe - O + h^+ \rightarrow Ti - Fe - O(h^+) \quad (3)$$

$$Ti - Fe - O(h^+) + e^- \rightarrow Ti - Fe - O^* \quad (4)$$

$$Ti - Fe - O^* \rightarrow Ti - Fe - O + h\nu \quad (5)$$

First, during a negative scan, $S_2O_8^{2-}$ is reduced at the Ti-Fe–O NTs electrode surface, and holes (h^+) are generated, as shown in Eqs. (1) and (2). The resulting h^+ is injected into the valence band of Ti-Fe–O (Eq. (3)). As the scanning potential develops in the negative direction, electrons fill the conduction band and generate the excited species Ti-Fe–O^* (Eq. (4)). Finally, when Ti-Fe–O^* returns from the excited state to the ground state, an ECL signal is emitted (Eq. (5)).

In this study, Ti-Fe–O NTs were selected to modify electrodes, resulting in excellent ECL performance. CCB/MNPs were used as quenchers to suppress the Ti-Fe–O NTs signal. Therefore, an ultrasensitive ECL biosensor was fabricated to detect a CYFRA21-1 cell marker.

ECL detection of CYFRA21-1

In this paper, we selected CYFRA21-1 as an antigen for analysis and investigated the potential of using Ti-Fe–O NTs as ECL electrode materials and CCB/MNPs as quenchers. Figure S4 shows the change in the ECL signal when detecting 100 ng·mL^{-1} CYFRA21-1 with different quenchers. Curves (a) and (b) show that the ECL strength decreased by 20% after CYFRA21-1 was assembled on the Ti-Fe–O NTs electrode. The main reason for this result was that CYFRA21-1 partially hindered electron transfer during the ECL reaction process. When the CYFRA21-1/Ab1/Ti-Fe–O NTs electrode was immersed in the Ab2/CCB/MNPs solution, the ECL signal was quenched by 89% (curve c). However, when the electrode assembled with CYFRA21-1

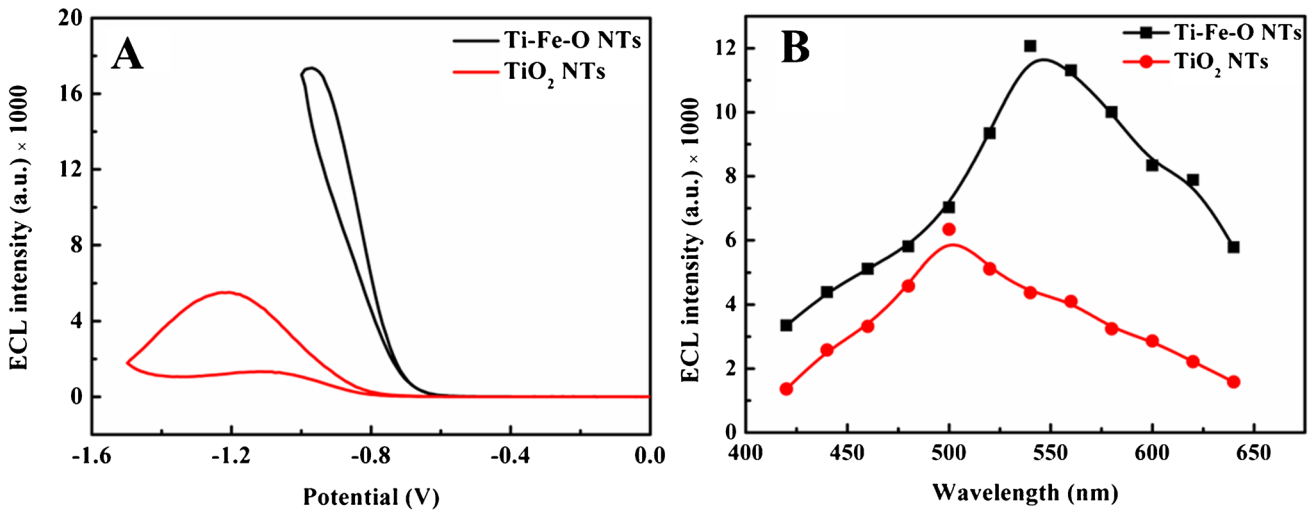

Fig. 2 **a** ECL curves of the Ti-Fe–O NTs electrode and TiO_2 NTs electrode. **b** The ECL spectrum of the Ti-Fe–O NTs and TiO_2 NTs electrode

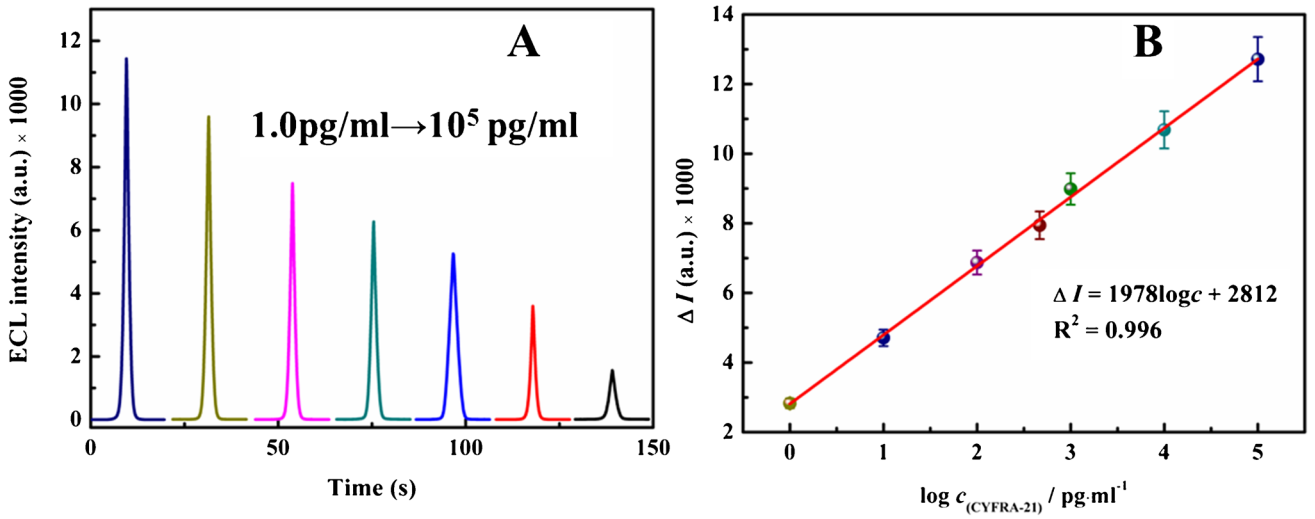

Fig. 3 **a** The ECL curves of Ti-Fe–O NTs in different concentrations of CYFRA21-1. **b** Logarithmic calibration curve for CYFRA21-1 detection

only combined with Ab2/MNPs, the ECL signal was only quenched by 42% (curve d). A comparative analysis of the results shows that only the combination of CCB and MNPs achieved effective quenching. Therefore, CCB/MNPs were selected as quenchers for subsequent experiments.

In this paper, the obtained biosensor uses the ECL method to detect different concentrations of CYFRA21-1, and the results are shown in Fig. 3. It can be clearly seen from Fig. 3a that as the concentration of CYFRA21-1 increases from 1 pg·mL^{-1} to 100 ng·mL^{-1}, the intensity of ECL gradually increases. Figure 3b is showing the relationship between the logarithm of the concentration of CYFRA21-1 and ΔI. The linear regression equation $\Delta I = 1978 \log c + 2812$ ($R^2 = 0.996$), where ΔI is I_0-I, I_0 is the ECL intensity of the electrode after incubation in CYFRA21-1 solution, and I is the ECL intensity of CYFRA21-1/Ab1/Ti-Fe–O NTs electrode. In addition, the detection limit of detection (LOD) was 0.114 pg·mL^{-1}.

Stability, repeatability, and selectivity

The prepared biosensor was maintained at 4 °C for 5 days. The result is shown in Fig. S5A, that is, the ECL curve of Ti-Fe–O NTs hardly changes in intensity over 5 days. This result indicates that the prepared ECL sensor had high stability. Figure S5B shows the results of a repeatability test performed on 5 different Ti-Fe–O NTs electrodes. The ECL

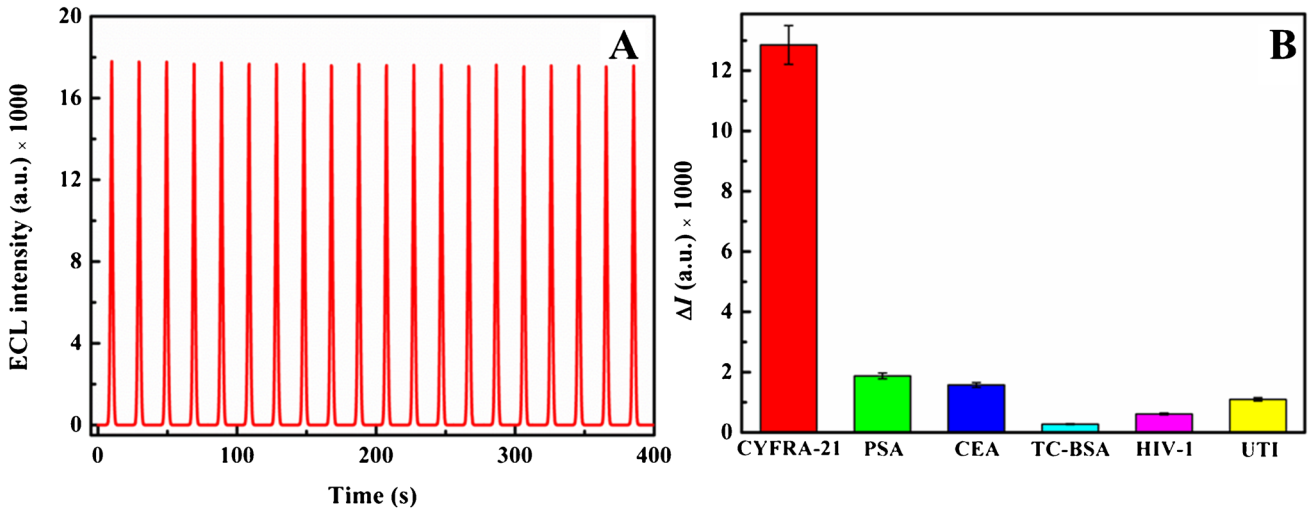

Fig. 4 **a** ECL behavior of Ti-Fe–O NTs in PBS (0.1 M, pH = 7.4) containing 0.05 M $K_2S_2O_8$. **b** Selectivity of the obtained ECL biosensor incubated in PSA, CEA, TC-BSA, HIV-1, and UTI for CYFRA21-1 under the same experimental conditions

Table 1 Comparison of different methods for detecting CYFRA21-1

Method	Linear range ($ng \cdot mL^{-1}$)	Detection limit ($pg \cdot mL^{-1}$)	Reference
Electrochemistry	0.25 ~ 800	100	[30]
Fluorescence	0.003 ~ 300	2.34	[31]
Chemiluminescence	0.1 ~ 1000	76.0	[32]
Electrochemistry	0.5 ~ 200	180	[33]
ECL	0.001 ~ 100	0.114	This work

strength of the 5 electrodes was almost stable, proving that the titanium ferrite electrode had good repeatability.

Figure 4a shows that Ti-Fe–O NTs generated strong and stable ECL signals. We investigated the selectivity of the CYFRA21-1 ECL biosensor. Under fixed detection conditions, we selected interfering proteins, including PSA, CEA, UTI, TC-BSA, and HIV-1 (at a 100 $ng \cdot mL^{-1}$ concentration), for detection. The results are shown in Fig. 4b: the interfering substances had almost no effect on the ECL biosensor, indicating that the biosensor had particularly good selectivity. Finally, we compared the performance of ECL methods that have been used to detect CYFRA21-1 over the past few years, and the results are shown in Table 1. The results show that our prepared biosensor for detecting CYFRA21-1 has a larger detection range and lower LOD than other detection methods.

Detection of real samples

In order to verify the practicability of real samples, the standard addition method is used to complete the relevant detection. The Affiliated Hospital of Yantai University provides serum with 0.5 $ng \cdot mL^{-1}$ of CYFRA21-1 in healthy students. Then, different concentrations of CYFRA21-1 (0.1 $ng \cdot mL^{-1}$, 1 $ng \cdot mL^{-1}$, 10 $ng \cdot mL^{-1}$) were added to the serum, and the mixture was used as the target for detection. Table 2 shows that the recoveries of CYFRA21-1 in actual samples ranged from 88.6 to 104.4%, and the RSD was below 3.0%. The results showed that the biosensor can be effectively applied to detect CYFRA21-1 in serum.

Table 2 Standard addition data of purposed biosensor for CYFRA21-1 detection

Orign numer ($ng \cdot mL^{-1}$)	Spiked samples ($ng \cdot mL^{-1}$)	Found ($ng \cdot mL^{-1}$)	Recovery (%)	RSD (%)
0.5	0.0	0.443	88.6	3.0
0.5	0.1	0.616	102.7	1.8
0.5	1	1.548	103.2	1.4
0.5	10	10.964	104.4	2.3

Conclusions

In this paper, the properties and applications of Ti-Fe–O-NTs electrodes were investigated using the ECL method. The Ti-Fe–O NTs electrode has high sensitivity and stable ECL signal. However, compared with the common glassy carbon electrode, the preparation process of this electrode is more complicated, takes longer, and needs to be stored at 4 °C. The Ti-Fe–O NTs electrode was used to generate the ECL signal, and a CCB/MNP complex was quenched with high efficiency to design a sandwich immunosensor for CYFRA21-1 detection, with the LOD being 0.114 $pg \cdot mL^{-1}$. The fabricated biosensor was applied to the detection of CYFRA21-1 in human serum, and satisfactory results were obtained. This result indicated the good potential of the biosensor prepared in this study for practical applications.

Supplementary Information The online version contains supplementary material available at https://doi.org/10.1007/s00604-022-05239-z.

Funding This work was financially supported by the National Natural Science Foundation of China (21778047), and the Natural Science Foundation of Shandong Province (grant no. ZR2021MB024).

Declarations

Conflict of interest The authors declare no competing interests.

References

1. Bai J, Zhou B-X (2014) Titanium dioxide nanomaterials for sensor applications. Chem Rev 114:10131–10176
2. Nozik A-J (1983) Photoelectrochemical cells. Nature 414:338–344
3. Konstantinou I-K, Albanis T-A (2004) TiO_2-Assisted photocatalytic degradation of azo dyes in aqueous solution: kinetic and mechanistic investigations: a review. Appl Catal B-Environ 49:1–14
4. Meng N, Leung M, Leung D, Sumathy K (2007) A review and recent developments in photocatalytic water-splitting using TiO_2 for hydrogen production. Renew Sust Energ Rev 11:401–425
5. Mills A, Hunte S-L (1997) An overview of semiconductor photocatalysis. J Atmos Chem 108:1–35
6. Oriol R, Sirés I, Brillas E, Andrade A-D (2019) A hybrid photoelectrocatalytic/photoelectro-Fenton treatment of Indigo Carmine in acidic aqueous solution using TiO_2 nanotube arrays as photoanode. J Electroanal Chem 847:113088
7. Yogi C, Kojima K, Takai T, Wada N (2009) Photocatalytic degradation of methylene blue by Au-deposited TiO_2 film under UV irradiation. J Mater Sci 44:821–827
8. Park J-Y, Hwang K-J, Lee J-W, Lee I-H (2011) Fabrication and characterization of electrospun Ag doped TiO_2 nanofibers for photocatalytic reaction. J Mater Sci 97:64–66
9. Yang L, Luo S, Liu R, Cai Q, Xiao Y, Liu S, Su F, Wen L (2010) Fabrication of CdSe nanoparticles sensitized long TiO_2 nanotube arrays for photocatalytic degradation of

anthracene-9-carbonxylic acid under green monochromatic light. J Phys Chem Lett 114:4783–4789
10. Guo J, Han Q, Zhong S, Zhu B, Huang W, Zhang S (2018) Au/M-TiO_2 nanotube catalysts (M=Ce, Ga Co, Y): preparation, characterization and their catalytic activity for CO oxidation. J Sol-gel Sci Technol 86:699–710
11. Chen Y, Tang W, Ma J, Ge B, Wang X, Wang Y, Ren P, Liu R (2020) Nickel-decorated TiO_2 nanotube arrays as a self-supporting cathode for lithium–sulfur batteries. Front Mater Sci 14:266–274
12. Qin X, Geng L, Wang Q, Wang Y (2019) Photoelectrochemical aptasensing of ofloxacin based on the use of a TiO_2 nanotube array co-sensitized with a nanocomposite prepared from polydopamine and Ag_2S nanoparticles. Microchim Acta 186:430
13. Su Y, Yang S, Liu W, Qiao L, Yan J, Liu Y, Zhang S, Fang Y (2017) Visible light photoelectrochemical sulfide sensor based the use of TiO_2 nanotube arrays loaded with Cu_2O. Microchim Acta 186:4065–4072
14. Wang W, Xie Y, Xia C, Du H, Tian F (2014) Titanium dioxide nanotube arrays modified with a nanocomposite of silver nanoparticles and reduced graphene oxide for electrochemical sensing. Microchim Acta 181:1325–1331
15. Akhavan O, Azimirad R (2009) Photocatalytic property of Fe_2O_3 nanograin chains coated by TiO_2 nanolayer in visible light irradiation. Appl Catal A-Gen 369:77–82
16. Mei Q, Zhang F, Wang N, Yang Y, Wu R, Wang W (2019) TiO_2/Fe_2O_3 heterostructures with enhanced photocatalytic reduction of Cr (VI) under visible light irradiation. RSC Adv 9:22764–22771
17. Sadeghi-Niaraki S, Ghasemi B, Habibolahzadeh A, Ghasemi E, Ghahari M (2019) Nanostructured $Fe_2O_3@TiO_2$ pigments with improved NIR reflectance and photocatalytic ability. Mater Chem Phys 235:121769
18. Zhang Y-N, Huang W-N, Zhang Y-J, Tang B, Xiao H-S, Zhao G-H (2016) Fabrication and enhanced visible-light photoelectrochemical performance of periodic hierarchical 3D Ti-Fe-O structure. Mater Lett 168:24–27
19. Lu H-X, Dai G-H, Dai R-H, Ding X, Liu M-C, Sun H-H, Sun C-Q, Zhao G-H (2019) Visible-light-driven photoelectrochemical aptasensor based on reduced graphene oxide/Ti-Fe-O nanotube arrays for highly sensitive and selective determination of microcystin-LR. Electrochim Acta 324:134820
20. Madian M, Wang Z, Gonzalez-Martinez I, Oswald S, Mikhailova D (2020) Ordered Ti-Fe-O nanotubes as additive-free anodes for lithium ion batteries. Appl Mater Today 20:100676
21. Gui G, Zhuo Y, Chai Y-Q, Liao N, Zhao M, Han J, Zhu Q, Yuan R, Xiang Y (2013) Supersandwich-type electrochemiluminescenct aptasensor based on $Ru(phen)_3^{2+}$ functionalized hollow gold nanoparticles as signal-amplifying tags. Biosens Bioelectron 47:524–529
22. Ml A, Cw A, Lc A, Dla B (2019) A novel electrochemiluminescence sensor based on resonance energy transfer system between nitrogen doped graphene quantum dots and boron nitride quantum dots for sensitive detection of folic acid. Anal Chim Acta 1090:57–63
23. Zhai Q-F, Li J, Wang E-K (2017) Recent advances based on nanomaterials as electrochemiluminescence probes for the fabrication of sensors. ChemElectroChem 4:1639–1650
24. Siegel R-L, Miller K-D, Jemal A (2020) Cancer statistics, 2020. CA Cancer J Clin 70:7–30
25. Wieskopf B, Demangeat C, Purohit A, Stenger R, Gries P (1995) Cyfra 21–1 as a biologic marker of non-small cell lung cancer: evaluation of sensitivity, specificity, and prognostic role. Chest 108:163–169
26. Rui H-X, Chang Z-L, Yi L, Wen L-X, Wen B-Y (2015) Optimal cut-off values for CYFRA 21–1 expression in NSCLC patients depend on the presence of benign pulmonary diseases. Clin Chim Acta 440:188–192
27. Tian C-Y, Xu J-J, Chen H-Y (2012) A novel aptasensor for the detection of adenosine in cancer cells by electrochemiluminescence of nitrogen doped TiO_2 nanotubes. Chem Commun 48:8234–8236
28. Zhang Q, Yu L, Xu C, Zhang W, Diao G (2020) A novel method for facile preparation of recoverable $Fe_3O_4@TiO_2$ core-shell nanospheres and their advanced photocatalytic application. Chem Phys Lett 761:138073
29. Dai P, Ke J, Xie C, Wei L, Jin J (2020) An off–on electrochemiluminescence detection for microRNAs based on TiO_2 nanotubes sensitized with gold nanoparticles as enhanced emitters. Anal Bioanal Chem 412:5779–5787
30. Zeng Y, Bao J, Zhao Y-N, Huo D-Q, Chen M (2018) A sensitive label-free electrochemical immunosensor for detection of cytokeratin 19 fragment antigen 21–1 based on 3D graphene with gold nanopaticle modified electrode. Talanta 178:122–128
31. Wang X, Zhang Y, Zhao L, Zhao D, Wang H, Yang J (2020) Polysaccharide-enhanced ARGET ATRP signal amplification for ultrasensitive fluorescent detection of lung cancer CYFRA 21–1 DNA. Anal Bioanal Chem 412:2413–2421
32. Wang Y-X, Guo X-Y, Liu J-W, Weng Z-X, Chen Y-X (2018) Development of chemiluminescent microparticle immunoassay for cytokeratin 19 fragment 21–1 content. Chin J Biologic 31:523–527
33. Yang H, Bao J, Huo D, Zeng Y, Hou C (2020) Au doped polythionine and poly-m-Cresol purple: Synthesis and their application in simultaneously electrochemical detection of two lung cancer markers CEA and CYFRA21–1. Talanta 224:121816